Bio-Design and Manufacturing (2019) 2:172–180
https://doi.org/10.1007/s42242-019-00043-w

RESEARCH ARTICLE

Liquid-phase 3D bioprinting of gelatin alginate hydrogels: influence of printing parameters on hydrogel line width and layer height

Maha Alruwaili[1,2] · Jose A. Lopez[1,3] · Kevin McCarthy[1,2] · Emmanuel G. Reynaud[1,3] · Brian J. Rodriguez[1,2]

Received: 15 June 2019 / Accepted: 4 July 2019 / Published online: 16 July 2019

Abstract

Extrusion-based 3D bioprinting is a direct deposition approach used to create three-dimensional (3D) tissue scaffolds typically comprising hydrogels. Hydrogels are hydrated polymer networks that are chemically or physically cross-linked. Often, 3D bioprinting is performed in air, despite the hydrated nature of hydrogels and the potential advantage of using a liquid phase to provide cross-linking and otherwise functionalize the hydrogel. In this work, we print gelatin alginate hydrogels directly into a cross-linking solution of calcium chloride and investigate the influence of nozzle diameter, distance between nozzle and surface, calcium chloride concentration, and extrusion rate on the dimensions of the printed hydrogel. The hydrogel layer height was generally found to increase with increasing extrusion rate and nozzle distance, according to the increased volume extruded and the available space, respectively. In addition, the hydrogel width was generally found to increase with decreasing nozzle distance and cross-linking concentration corresponding to confinement-induced spreading and low cross-linking regimes, respectively. Width/height ratios of ~ 1 were generally achieved when the nozzle diameter and distance were comparable above a certain cross-linking concentration. Using these relationships, biocompatible 3D multilayer structures were successfully printed directly into calcium chloride cross-linking solution.

Keywords Gelatin alginate · Hydrogel · Additive manufacturing · 3D printing · 3D bioprinting · Biomaterials · Extrusion · Bioplotting

Introduction

Additive manufacturing by extrusion-based three-dimensional (3D) bioprinting enables the direct deposition of biomaterials for the fabrication of 3D scaffolds [1–3]. The potential applications of 3D bioprinting span from regenerative medicine to tissue engineering [4–6]. Ideally, 3D bioprinting will enable the creation of biocompatible 3D scaffolds with tailored physical, chemical, and biological functionality [7]. Such scaffolds should be made of generally soft biopolymer hydrogels prepared with stiffness suitable for the cell line to be investigated [3, 8]. Notably, extrusion-based 3D bioprinting is typically performed in air, which places limits on the types of materials that can be printed [3, 7, 9–13]. The dimensions of a printed hydrogel and the print resolution, defined as the width and height of a single line, depend strongly on the hydrogel used and on the printing parameters nozzle diameter, distance between nozzle and surface (i.e., nozzle distance), and extrusion rate [14–17], as annotated in Fig. 1. As hydrogels are hydrated 3D polymer networks that are cross-linked by chemical or physical interactions, it is important to cross-link bioprinted hydrogels to maintain their structure and keep bioprinted hydrogels in a liquid environment so as to avoid the detrimental effects of dehydration [18–20]. Several strategies have been employed to ionically cross-link extruded hydrogels, including cross-linking a structure post-printing [21], lowering the print into cross-linking solution during printing [22], coaxial/microfluidic print head designs

Electronic supplementary material The online version of this article (https://doi.org/10.1007/s42242-019-00043-w) contains supplementary material, which is available to authorized users.

✉ Emmanuel G. Reynaud
emmanuel.reynaud@ucd.ie

✉ Brian J. Rodriguez
brian.rodriguez@ucd.ie

1 Conway Institute of Biomolecular and Biomedical Research, University College Dublin, Dublin, Ireland

2 School of Physics, University College Dublin, Dublin, Ireland

3 School of Biomolecular and Biomedical Science, University College Dublin, Dublin, Ireland

to cross-link during extrusion [23, 24], cross-linking during printing using an aerosol system [25], pre-cross-linking the hydrogel prior to extrusion [26], among others [27]. In another strategy, first reported in 2000 as 3D plotting or 3D bioplotting, extrusion of materials (e.g., moisture curable silicone resin, alginate, agar, agarose, and gelatin) is performed directly in cross-linking solution (Fig. 1) on a submerged, often roughened, print surface [28–31]. Printing in non-reactive support solutions and gels has also been demonstrated [32–34]. While examples of printing alginate-based hydrogels directly into cross-linking exist [29, 35–39] and scaffolds printed in cross-linking solution were reported to improve printing outcomes [39] and cell viability [36] compared to printing in air, experiments have typically been performed using only one nozzle diameter and one cross-linking solution [29, 35–37, 39]. Furthermore, typically the width, but not the layer height, of the printed hydrogels is reported, the influence of extrusion rate is not investigated, and the nozzle distance is not mentioned or kept constant. Compared to printing in air, printing into a cross-linking solution brings additional challenges, such as swelling, and understanding the influence of printing parameters on print dimensions and resolution becomes crucial for the fabrication of 3D scaffolds. For example, the choice of nozzle distance for the second layer requires knowledge of the first layer height. In this work, we print biocompatible [40, 41] and biodegradable [42, 43] gelatin alginate hydrogels directly into a cross-linking solution of calcium chloride ($CaCl_2$). By investigating the influence of nozzle diameter, nozzle distance, $CaCl_2$ concentration, and extrusion rate on the dimensions of the printed hydrogel, a parameter space for printing multilayer structures was identified and successfully demonstrated. This work provides a strategy for testing hydrogels for liquid-phase 3D bioprinting, which may expand the types of hydrogels that can be used in extrusion-based 3D bioprinting, and allow the fabrication of 3D scaffolds that provide an environment similar to the in vivo extra cellular matrix for tissue engineering and drug toxicity applications.

Materials and methods

Gelatin alginate

To prepare gelatin alginate hydrogels, gelatin (0.06 g/ml type B, Sigma-Aldrich) and sodium alginate (0.05 g/ml type P1, Sigma-Aldrich) powders were mixed using a magnetic stirrer at 200 rpm in deionized water at 65 °C for 10 min. Typically, 3 g of gelatin and 2.5 g of alginate were added to 50 ml of deionized water and 0.01 g of orange food dye (U8-OSL0-PS8Q, Preema) was added during mixing to better visualize the nominally transparent printed structures. The heated hydrogel was loaded into a 20 ml sterile syringe with Luer lock tip (BDAM302237, VWR) prior to printing.

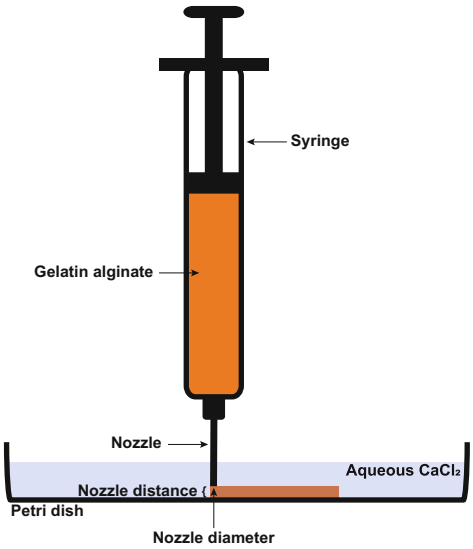

Fig. 1 Schematic of a syringe extruding gelatin alginate hydrogel onto a support in liquid; nozzle diameter is the inner diameter of the nozzle and nozzle distance is the separation between the end of the nozzle and the print surface

Cross-linking solution

Calcium chloride ($CaCl_2$) powder (MFCD00149613, Fisher Scientific) was dissolved in deionized water to prepare cross-linking solutions with concentrations of 20–160 mM.

3D bioprinting

An Ultimaker Original 3D printer was modified to enable syringe-based extrusion, as shown in Fig. 2. The syringe holder consisted of polylactic acid parts 3D printed on an Ultimaker 3. The parts were used (1, 2) to hold the stepper motor (SM42HT38-1684AL, Smart Automation Motor Manufacturing Co., Ltd.), (3) to interface with the lead screw, and (4) to replace the syringe plunger [(5) a plunger cap (15889152, Fisher Scientific) was affixed to the end of the printed plunger], and (6) mount the syringe, as shown schematically in Fig. 2a, b and fully assembled in Fig. 2c. In this manner, syringe extrusion was controlled by the stepper motor using even numbered extrusion rates in the range 6–24 mm/s. For reference, 12 mm/s corresponds to an extrusion rate of ~0.04 ml/s for the gelatin alginate hydrogel prepared. The print head speed in x and y was kept constant at 2 mm/s, within the 1–10 mm/s range typically reported for bioprinting [44]. The hydrogel temperature was maintained at 65 °C using a self-adhesive heating element (PPI Adhesive Products Limited) wrapped around (7) an aluminum cylinder holding (8) a 20 ml plastic syringe (15889152, Fisher Scien-

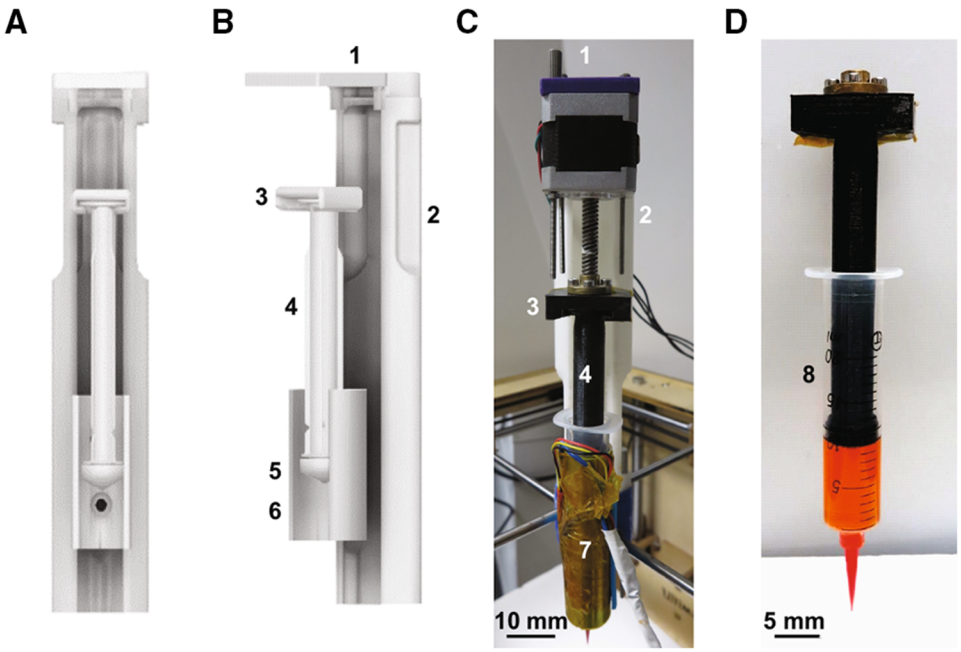

Fig. 2 **a**, **b** Representations of the bespoke syringe holder from two perspectives. **c** Photograph of the entire print head. **d** 20 ml Syringe filled with 10 ml of gelatin alginate hydrogel with orange dye

tific), as shown in Fig. 2d, and controlled using an Arduino Uno (not shown). Plastic tapered dispensing needles (Somerset Solders Ltd) with inner nozzle diameters of 0.58 mm, 0.84 mm, 1.20 mm, and 1.60 mm were used in this work.

Prior to printing, a 90 mm diameter Petri dish lid (Fisher Scientific) was sanded (80-grit sandpaper, ZG-02-SZ-80, ZesGood) to roughen the surface and promote print attachment. 2 ml of $CaCl_2$ cross-linking solution was then placed in the plastic petri dish. One layer comprising 4 connected lines, 40 mm in length and separated by 4 mm, was then printed using nozzle distances of 0.3, 0.5, and 0.8 mm, $CaCl_2$ concentrations of 20–160 mM within the range of typical $CaCl_2$ values [45], and previously described extrusion rates and nozzle diameters. One layer comprising 10 connected lines, 60 mm in length and separated by 4 mm, each printed with a different extrusion rate between 6 and 24 mm/s, was also used (e.g., Figure S1).

Preliminary attempts at printing established that if the distance between the nozzle and the substrate was too large, the printed gel would not adhere to the substrate, and that if the distance was too small, the hydrogel would not exit the nozzle. Within these extremes and depending on the parameters selected, it is reasonable to expect, under the chosen conditions, that the cross section of a single printed line would have a geometry similar to one of the three categories shown in Fig. 3: where (i) the width is roughly equal to the height (width/height ratio less than 1.3), (ii) the width is greater than the height (width/height ratio greater than or equal to 1.3 and less than or equal to 2), or (iii) the width is more than twice the height. The category height/width ratios are defined quantitatively only for classification purposes; however, qualitatively, they are intended to identify shapes

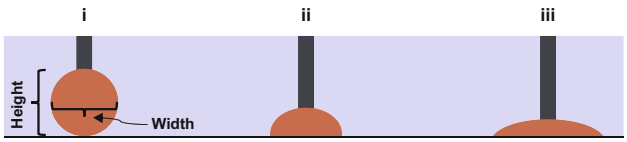

Fig. 3 Schematic showing the height and width of the structure printed into $CaCl_2$ cross-linking solution and three possible printing outcomes or categories depending on print parameters used: (i) width/height ratio less than 1.3, (ii) width/height ratio greater than or equal to 1.3 and less than or equal to 2, and (iii) the width is more than twice the height

that might be suitable for multilayer stacking or fusion [17], depending on cross-linking concentration. Understanding the relationships between printing parameters and printed line geometry is a critical first step toward the fabrication of multilayer objects printed in a cross-linking solution.

Optical characterization

After printing and after cross-linking for 10 min, the printed hydrogel layer was sliced with a scalpel (Steel Blade) from the middle, gently removed from the petri dish using tweezers (Round Tip Micro Tweezers 160 mm, Nizbets), and placed on a glass slide for imaging (e.g., Figure S2). To image the dimensions of the hydrogel (line height and width determined as mean and standard deviation from 10 measurements each), a camera (P/S G1X II, Canon) was used. A cross-linking time of 10 min was chosen to reflect a reasonable time between printing subsequent layers and to minimize the effect of swelling behavior across a broad concentration range (Figure S3).

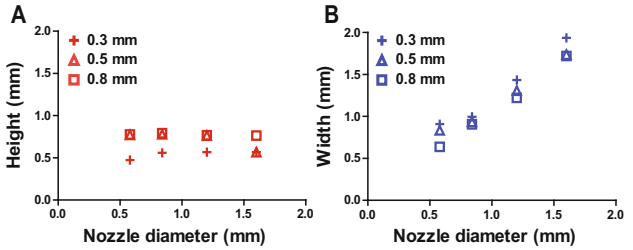

Fig. 4 **a** Height and **b** width of gelatin alginate hydrogels printed into 60 mM $CaCl_2$ using nozzle distances of 0.3, 0.5, and 0.8 mm, an extrusion rate of 12 mm/s, and nozzle diameters of 0.58, 0.84, 1.20, and 1.60 mm

Results and discussion

Influence of nozzle diameter and nozzle-surface distance

As in any fused filament fabrication or direct deposition approach, nozzle diameter and distance are key parameters that essentially define print resolution and layer height, respectively. Given the importance of these parameters, their influence on print dimensions in cross-linking solution was investigated specifically in a liquid-phase bioprinting setup. Average height and widths of gelatin alginate hydrogel lines printed using an extrusion rate of 12 mm/s into a 60 mM $CaCl_2$ solution for nozzle distances of 0.3, 0.5, and 0.8 mm which are typical values for 3D bioprinting [46, 47] with the nozzle diameters used: 0.58, 0.84, 1.20, and 1.60 mm are shown in Fig. 4. Nozzle distances of 0.3 and 0.5 mm yielded hydrogels of height slightly greater than the nozzle distance. The heights were generally independent on nozzle diameter (Fig. 4a). Under these conditions, the hydrogel height was generally initially confined by nozzle distance and likely swelled as the nozzle moved away along the printing path. The height for a nozzle distance of 0.8 mm was the same as for 0.5 mm (~0.75 mm regardless of nozzle diameter). Given that the widths are also similar under these conditions, it is likely that for the extrusion rate and print head speed selected, the volume extruded is insufficient for the hydrogel height to be affected by the nozzle distance at 0.5 mm and above. The hydrogel widths increased linearly with increasing nozzle diameter for all distances (Fig. 4b). Due to the smaller than nozzle diameter distance, the hydrogel expanded laterally during extrusion at the concentration and extrusion rate used, resulting in a width that increased with increasing nozzle diameter that was slightly larger than the nozzle diameter.

The data plotted in Fig. 4, available in Supporting Information as Table S1, was also plotted as a function of distance instead of nozzle diameter, as shown in Figure S4. From these representations, we concluded that the height values generally increased with increasing distance whereas width values generally decreased with increasing distance for all nozzle diameters investigated, in agreement with the trends identified from Fig. 4. Similar behavior was observed for hydrogels printed into 80 mM and 100 mM $CaCl_2$, as shown in Figure S5 and Table S2 and Figure S6 and Table S3, respectively.

Table 1 Dependence on nozzle diameter and distance for a $CaCl_2$ concentration of 60 mM and an extrusion rate of 12 mm/s of the ratio of the width to the height of the printed hydrogel structures

Nozzle diameter (mm)	Distance (mm)	Width/height ratio	Category
0.58	0.3	1.48 ± 0.02	(ii)
	0.5	0.84 ± 0.01	(i)
	0.8	0.82 ± 0.02	(i)
0.84	0.3	1.76 ± 0.02	(ii)
	0.5	1.20 ± 0.05	(i)
	0.8	1.13 ± 0.02	(i)
1.2	0.3	2.50 ± 0.05	(iii)
	0.5	1.71 ± 0.05	(ii)
	0.8	1.31 ± 0.01	(ii)
1.6	0.3	3.45 ± 0.02	(iii)
	0.5	2.30 ± 0.07	(iii)
	0.8	2.24 ± 0.01	(iii)

For the largest nozzle diameters (1.2 and 1.6 mm), the prints generally fall into category (iii) of Fig. 3; however, for nozzle distances of 0.5 and 0.8 mm for the 1.2 mm nozzle diameter, the ratios of width to height are less than 2 (Table 1), falling into category (ii). For nozzle diameters of 0.84 and 0.58 mm, the prints are close to category (i) except for the smallest nozzle distance (0.3 mm), which leads to category (ii) prints. Notably, whereas the ratios of the two 0.84 mm category (i) prints are greater than 1, the ratios of the two 0.58 mm category (i) prints are less than 1. Ratios less than 1 likely result when the distance is roughly equal to or greater than the nozzle diameter. The closest agreement between nozzle diameter and hydrogel height and width was obtained for a nozzle diameter of 0.84 mm and a distance of 0.8 mm, which resulted in a hydrogel having a height of 0.78 ± 0.02 mm and a width of 0.88 ± 0.01 mm (1.13 ± 0.02 mm width/height ratio); however, such agreement is expected to depend strongly on the cross-linking concentration used.

Influence of cross-linking concentration

While similar print dimensions were obtained for hydrogels printed into 60–100 mM $CaCl_2$, (Figs. 4, S5, S6) it is necessary to further characterize the influence of cross-linking concentration across a broader concentration range. Gelatin alginate hydrogels were printed into $CaCl_2$ concentrations in the range of 20–160 mM using a 12 mm/s extrusion rate as a

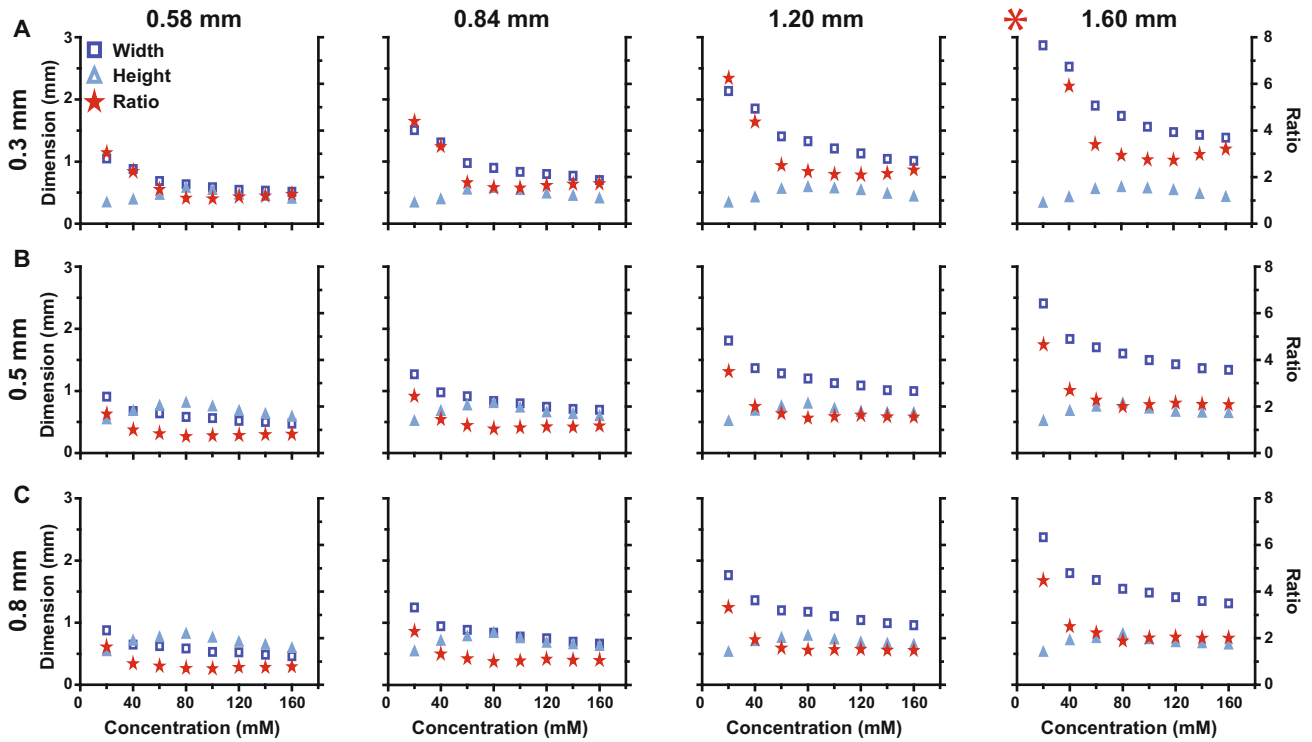

Fig. 5 Width, height, and width/height ratio of hydrogels printed into various $CaCl_2$ concentrations using nozzle distances of **a** 0.3 mm, **b** 0.5 mm, and **c** 0.8 mm, an extrusion rate of 12 mm/s, and nozzle diameters of 0.58, 0.84, 1.20, and 1.60 mm. In (**a**), as denoted with an asterisk, the data point for the ratio for 1.6 mm nozzle diameter at 20 mM is off the scale shown (8.46 ± 0.04). Data is provided in Tables S4–S15

function of nozzle diameter and distance and the dimensions (height, width, and ratio of width to height) of the resulting hydrogel structures were measured and plotted (Fig. 5).

For a nozzle distance of 0.3 mm and a nozzle diameter of 0.58 mm, hydrogel widths were greater than the heights for concentrations 60 mM and below (Fig. 5a). Above 60 mM, the heights and widths were similar, resulting in ratios of ~1, corresponding to category (i). The heights and widths were also comparable to the nozzle diameter. For larger nozzle diameters, low concentrations also resulted in hydrogel widths greater than the heights. As the nozzle distance was smaller than the nozzle diameter in Fig. 5a, the widths remained larger than the height for all concentrations. It was not possible to achieve a category (i) print for larger nozzle diameters for a nozzle distance of 0.3 mm; however, the ratio is closest to 1 at intermediate concentrations corresponding also to conditions when the widths were comparable to the nozzle diameters.

For a nozzle distance of 0.5 mm and nozzle diameters of 0.58 mm and 0.84 mm, hydrogel widths and heights were comparable, and ratios close to 1 were achieved at most concentrations, corresponding to category (i) (Fig. 5b). For larger nozzle diameters, widths were greater than heights, resulting in ratios > 1 and corresponding to categories (ii) and (iii).

For a 0.8 mm nozzle distance and a 0.58 mm nozzle diameter, heights were generally larger than widths, with ratios < 1 (Fig. 5c). For a 0.84 mm nozzle diameter, heights and widths were similar above 60 mM, with ratios close to 1. For the larger nozzle diameters, widths were larger than heights and category (i) prints could not be obtained.

The data shown in Fig. 5 highlights the interplay between nozzle distance and diameter and $CaCl_2$ concentration when printing gelatin alginate. At low concentrations, widths are generally larger than the nozzle diameter and heights are generally determined by the nozzle distance when the distance is less than the nozzle diameter; The gelatin alginate spreads out laterally with a low degree of cross-linking. When the nozzle distance is greater than the nozzle diameter, heights can be larger than widths except at the lowest cross-linking concentrations. From Fig. 5, category (i) prints with width/height ratios of ~1 appear most likely to occur when the nozzle diameter and distance have similar dimensions and the concentration is greater than 60 mM. Ratios of ~1 are possible to obtain when the nozzle distance is slightly smaller than the nozzle diameter (e.g., 0.3 mm and 0.58 mm, respectively) at concentrations that result in moderate swelling to offset the initial nozzle confinement. If the nozzle distance is significantly greater than the nozzle diameter, ratios < 1 can be

obtained. If the distance is significantly less than the diameter, ratios > 1 are generally expected. While these parameters allow the print geometry and therefore the print resolution and layer height to be tuned at an extrusion rate of 12 mm/s, the role of extrusion rate also needs to be investigated and understood.

Influence of extrusion rate

So far, all data were obtained from hydrogels printed with an extrusion rate of 12 mm/s. As extrusion rate defines the rate at which the hydrogel is extruded, and therefore the volume extruded in a given time, it is a key printing parameter to understand. In order to determine the influence of the extrusion rate on the hydrogel dimensions, the hydrogel was printed into $CaCl_2$ concentrations in the range of 20–100 mM with even numbered extrusion rates in the range 6–24 mm/s for a nozzle distance of 0.5 mm and nozzle diameters of 0.58, 0.84, 1.20, and 1.60 mm. As shown in Fig. 5, concentrations above 100 mM did not strongly affect the measured hydrogel print dimensions. For a given nozzle diameter, increasing the extrusion rate increased the volume of hydrogel extruded. From Fig. 6, it is clear that the height and width generally increased linearly with increasing extrusion rate. A strong dependence on concentration was not observed, but the height and more so the width were generally slightly larger for lower concentrations. Given the linear dependence of the height and width on extrusion rate, it is reasonable to expect that plots such as in Fig. 5, obtained at different extrusion rates, could be used to determine which parameters can be used to produce a print of desired line geometry, print resolution, and layer height.

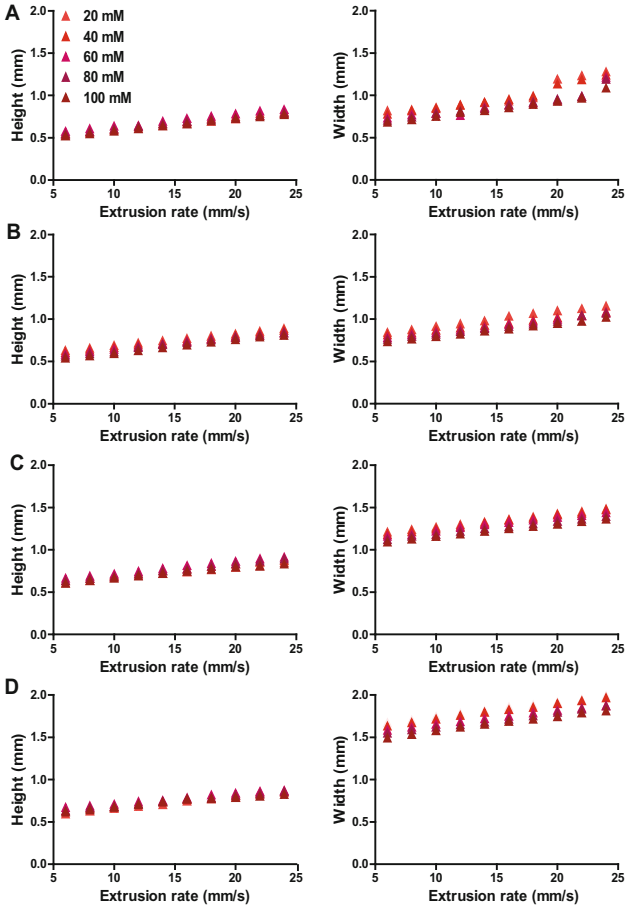

Fig. 6 Height and width of gelatin alginate hydrogels printed with different extrusion rates (6–24 mm/s) and concentrations (20–100 mM) using a nozzle distance of 0.5 mm and nozzle diameters of **a** 0.58 mm, **b** 0.84 mm, **c** 1.20 mm, and **d** 1.60 mm. Data is provided in Tables S16–S23

3D bioprinting of multilayer structures

The data presented above effectively maps the printing parameter space and allows us to select or predict the dimensions of the printed hydrogel and to choose appropriate nozzle distances for subsequent layers. Based on the expected line height and width for printing parameters discussed above, we printed 4-layer structures with different nozzle diameters into 60 mM $CaCl_2$ with an extrusion rate of 12 mm/s (Fig. 7). The initial and subsequent nozzle distances were chosen according to Table S1, as indicated in Table 2. Each layer was printed in ~4 s with no delay between subsequent layers.

Initial nozzle distances of 0.3 mm and subsequent nozzle distances of 0.5 mm were chosen for all nozzle diameters; the first layers were expected to be ~0.55 mm in height and subsequent layers were expected to be ~0.75 mm in height. The final height of the 4-layer structures was therefore expected to be in the range of 2–3 mm. As shown in Table 2, the final structure height was 2.60–2.70 mm and the overall average layer height was 0.67 ± 0.02 mm. For each of the nozzle diameters used, it was possible to obtain a multilayer structure with similar overall height and tunable line widths that depend on the nozzle diameter, concentration, and extrusion rate used, demonstrating the potential of liquid-phase 3D bioprinting. Similar 2-layer prints were found to be biocompatible; human mesenchymal stem cell viability was assessed using an Alamar Blue assay (DAL1025, Thermo Fisher) over 7 days relative to an empty well plate on grid structures printed using an extrusion rate of 12 mm/s, a nozzle diameter of 0.84 mm, and first and second layer nozzle distances of 0.3 mm and 0.5 mm, respectively, in 60 mM and 100 mM $CaCl_2$ cross-linking solution (Figure S7). Stem cells were seeded onto the prints after printing, as shear stress during extrusion can lead to cell death [37] and stem cell differentiation is particularly sensitive to mechanical factors [48].

The results presented here provide a simple guide for testing new hydrogels for liquid-phase 3D bioprinting. Char-

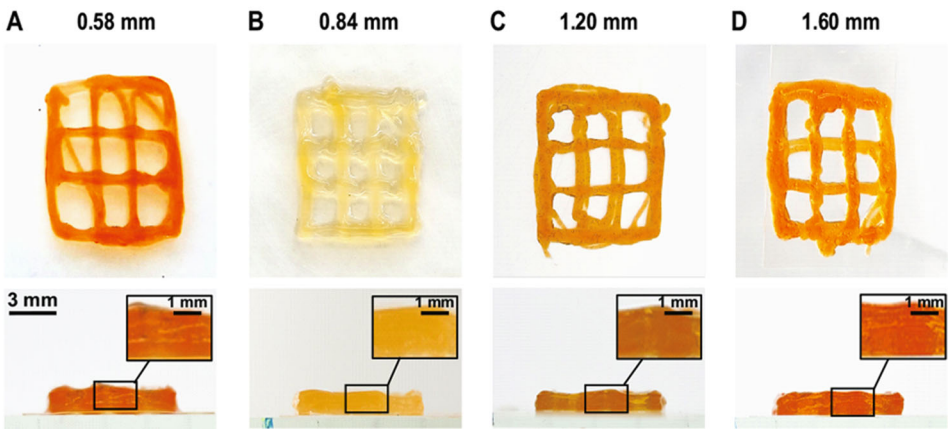

Fig. 7 Multilayer gelatin alginate hydrogel structures printed into a 60 mM $CaCl_2$ solution with an extrusion rate of 12 mm/s, and nozzle diameters of **a** 0.58 mm, **b** 0.84 mm, **c** 1.20 mm, and **d** 1.60 mm

Table 2 Chosen parameters for multilayer gelatin alginate hydrogel structures printed into a 60 mM $CaCl_2$ solution with an extrusion rate of 12 mm/s and resulting structure dimensions

Nozzle diameter	Expected initial layer height	Expected line width	Structure height	Structure line width
0.58	0.46 ± 0.01	0.68 ± 0.02	2.70 ± 0.03	0.67 ± 0.07
0.84	0.55 ± 0.02	0.97 ± 0.01	2.70 ± 0.04	0.98 ± 0.06
1.20	0.56 ± 0.01	1.40 ± 0.05	2.60 ± 0.06	1.20 ± 0.08
1.60	0.55 ± 0.02	1.90 ± 0.01	2.67 ± 0.05	1.60 ± 0.10

The first layer was printed using a nozzle distance of 0.3 mm; subsequent layers were printed with a nozzle distance of 0.5 mm. All values have units of mm

acterizing the effect of printing parameters on the geometry of the resulting hydrogel layer provides critical information relating to the selection of nozzle distance for subsequent layers. Notably, a variable nozzle distance may be required in order to obtain certain multilayer structures, depending on the hydrogel used and the printing parameters. In this work, control over line width and structure geometry is demonstrated, however, liquid-phase 3D bioprinting into cross-linking solution is expected to provide hydrogels with tunable mechanical properties as well [49], making it an attractive approach for generating tissue culture scaffolds with tunable functional properties.

Conclusions

Liquid-phase 3D bioprinting requires careful consideration of the print parameters: nozzle distance, nozzle diameter, cross-linking concentration, and extrusion rate. Proper selection of these parameters can allow the geometry of gelatin alginate hydrogel prints to be tuned, from lines with a ribbon-like geometry, where the width is larger than the height, to structures with width/height ratios of ~1. At low cross-linking concentrations, widths are generally larger than heights. When the nozzle distance is much less than the nozzle diameter, the printed structure, confined by the nozzle, expands laterally. Width/height ratios of ~1 are generally achieved when the nozzle diameter and distance are comparable above a certain cross-linking concentration. Print speed is another important parameter [17, 45], and the approach described should be undertaken each time a different print speed is used. This approach can be generalized and applied to other gels for liquid-phase 3D bioprinting prior to attempting multilayer prints. 3D bioprinting in liquid allows hydrogel prints to remain fully hydrated during and after printing and to tune the properties of the print through choice of cross-linking concentration.

Acknowledgements This research was funded by the Ministry of Higher Education of Saudi Arabia under the King Abdullah Scholarship Program (IR10133), Enterprise Ireland (CF-2016-0389-P), the European Union's Horizon 2020 research and innovation program under Marie Skłodowska-Curie Grant Agreement No. 644175, and Science Foundation Ireland (13/TIDA/B2701). This project was co-funded by the European Regional Development Fund (ERDF) under Ireland's European Structural and Investment Funds Programmes 2014–2020.

Compliance with ethical standards

Conflict of interest The authors declare that there is no conflict of interest.

Ethical approval This study does not contain any studies with human or animal subjects performed by any of the authors.

References

1. Vaezi M, Seitz H, Yang S (2013) A review on 3D micro-additive manufacturing technologies. Int J Adv Manuf Technol 67:1721–1754. https://doi.org/10.1007/s00170-012-4605-2
2. Lozano R, Stevens L, Thompson BC, Gilmore KJ, Gorkin R, Stewart EM, Panhuis M, Romero-Ortega M, Wallace GG (2015) 3D printing of layered brain-like structures using peptide modified gellan gum substrates. Biomaterials 67:264–273. https://doi.org/10.1016/j.biomaterials.2015.07.022
3. Derakhshanfar S, Mbeleck R, Xu K, Zhang X, Zhong W, Xing M (2018) 3D bioprinting for biomedical devices and tissue engineering: a review of recent trends and advances. Bioact Mater 3:144–156. https://doi.org/10.1016/j.bioactmat.2017.11.008
4. Ker EDF, Nain AS, Weiss LE, Wang J, Suhan J, Amon CH, Campbell PG (2011) Bioprinting of growth factors onto aligned sub-micron fibrous scaffolds for simultaneous control of cell differentiation and alignment. Biomaterials 32:8097–8107. https://doi.org/10.1016/j.biomaterials.2011.07.025
5. Narayanan LK, Huebner P, Fisher MB, Spang JT, Starly B, Shirwaiker RA (2016) 3D-bioprinting of polylactic acid (PLA) nanofiber–alginate hydrogel bioink containing human adipose-derived stem cells. ACS Biomater Sci Eng 2:1732–1742. https://doi.org/10.1021/acsbiomaterials.6b00196
6. Mandrycky C, Wang Z, Kim K, Kim D-H (2016) 3D bioprinting for engineering complex tissues. Biotechnol Adv 34:422–434. https://doi.org/10.1016/j.biotechadv.2015.12.011
7. Murphy SV, Atala A (2014) 3D bioprinting of tissues and organs. Nat Biotechnol 32:773–785. https://doi.org/10.1038/nbt.2958
8. Pati F, Jang J, Ha D-H, Won Kim S, Rhie J-W, Shim J-H, Kim D-H, Cho D-W (2014) Printing three-dimensional tissue analogues with decellularized extracellular matrix bioink. Nat Commun 5:11. https://doi.org/10.1038/ncomms4935
9. Zhang B, Gao L, Ma L, Luo Y, Yang H, Cui Z (2019) 3D Bioprinting: a novel avenue for manufacturing tissues and organs. Engineering. https://doi.org/10.1016/j.eng.2019.03.009 **(in press)**
10. Vijayavenkataraman S, Yan WC, Lu WF, Wang CH, Fuh JYH (2018) 3D bioprinting of tissues and organs for regenerative medicine. Adv Drug Deliv Rev 132:296–332. https://doi.org/10.1016/j.addr.2018.07.004
11. Jiang T, Munguia-Lopez JG, Flores-Torres S, Kort-Mascort J, Kinsella JM (2019) Extrusion bioprinting of soft materials: an emerging technique for biological model fabrication. Appl Phys Rev. https://doi.org/10.1063/1.5059393
12. Kyle S, Jessop ZM, Al-Sabah A, Whitaker IS (2017) 'Printability' of candidate biomaterials for extrusion based 3D printing: state-of-the-art. Adv Healthc Mater 6:1–16. https://doi.org/10.1002/adhm.201700264
13. Gao T, Gillispie GJ, Copus JS, Seol YJ, Atala A, Yoo JJ, Lee SJ (2018) Optimization of gelatin–alginate composite bioink printability using rheological parameters: a systematic approach. Biofabrication 10:034106. https://doi.org/10.1088/1758-5090/aacdc7
14. Datta P, Barui A, Wu Y, Ozbolat V, Moncal KK, Ozbolat IT (2018) Essential steps in bioprinting: from pre- to post-bioprinting. Biotechnol Adv 36:1481–1504. https://doi.org/10.1016/j.biotechadv.2018.06.003
15. Kang KH, Hockaday LA, Butcher JT (2013) Quantitative optimization of solid freeform deposition of aqueous hydrogels. Biofabrication 5:035001. https://doi.org/10.1088/1758-5082/5/3/035001
16. Gao Q, Niu X, Shao L, Zhou L, Lin Z, Sun A, Fu J, Chen Z, Hu J, Liu Y, He Y (2019) 3D printing of complex GelMA-based scaffolds with nanoclay. Biofabrication 11:035006. https://doi.org/10.1088/1758-5090/ab0cf6
17. He Y, Yang F, Zhao H, Gao Q, Xia B, Fu J (2016) Research on the printability of hydrogels in 3D bioprinting. Sci Rep 6:1–13. https://doi.org/10.1038/srep29977
18. Naghieh S, Karamooz-Ravari MR, Sarker M, Karki E, Chen X (2018) Influence of crosslinking on the mechanical behavior of 3D printed alginate scaffolds: experimental and numerical approaches. J Mech Behav Biomed Mater 80:111–118. https://doi.org/10.1016/j.jmbbm.2018.01.034
19. Opdahl A, Koffas TS, Amitay-Sadovsky E, Kim J, Somorjai GA (2004) Characterization of polymer surface structure and surface mechanical behaviour by sum frequency generation surface vibrational spectroscopy and atomic force microscopy. J Phys: Condens Matter 16:R659–R677. https://doi.org/10.1088/0953-8984/16/21/R02
20. Tan Z, Parisi C, Di Silvio L, Dini D, Forte AE (2017) Cryogenic 3D printing of super soft hydrogels. Sci Rep 7:16293. https://doi.org/10.1038/s41598-017-16668-9
21. Ouyang L, Yao R, Zhao Y, Sun W (2016) Effect of bioink properties on printability and cell viability for 3D bioplotting of embryonic stem cells. Biofabrication 8:035020. https://doi.org/10.1088/1758-5090/8/3/035020
22. Tabriz AG, Hermida MA, Leslie NR, Shu W (2015) Three-dimensional bioprinting of complex cell laden alginate hydrogel structures. Biofabrication 7:045012. https://doi.org/10.1088/1758-5090/7/4/045012
23. Gao Q, He Y, Zhong Fu J, Liu A, Ma L (2015) Coaxial nozzle-assisted 3D bioprinting with built-in microchannels for nutrients delivery. Biomaterials 61:203–215. https://doi.org/10.1016/j.biomaterials.2015.05.031
24. Ma J, Wang Y, Liu J (2018) Bioprinting of 3D tissues/organs combined with microfluidics. RSC Adv 8:21712–21727. https://doi.org/10.1039/c8ra03022g
25. Ahn S, Lee H, Kim G (2013) Functional cell-laden alginate scaffolds consisting of core/shell struts for tissue regeneration. Carbohydr Polym 98:936–942. https://doi.org/10.1016/j.carbpol.2013.07.008
26. Chung JHY, Naficy S, Yue Z, Kapsa R, Quigley A, Moulton SE, Wallace GG (2013) Bio-ink properties and printability for extrusion printing living cells. Biomater Sci 1:763–773. https://doi.org/10.1039/c3bm00012e
27. Ozbolat IT (2017) Extrusion-based bioprinting. In: Ozbolat IT (ed) 3D Bioprinting. Elsevier, Amsterdam, pp 93–124. https://doi.org/10.1016/b978-0-12-803010-3.00004-4
28. Landers R, Mülhaupt R (2000) Desktop manufacturing of complex objects, prototypes and biomedical scaffolds by means of computer-assisted design combined with computer-guided 3D plotting of polymers and reactive oligomers. Macromol Mater Eng 282:17–21. https://doi.org/10.1002/1439-2054(20001001)282:1%3c17:AID-MAME17%3e3.0.CO;2-8
29. Landers R, Pfister A, Hübner U, John H, Schmelzeisen R, Mülhaupt R (2002) Fabrication of soft tissue engineering scaffolds by means of rapid prototyping techniques. J Mater Sci 37:3107–3116. https://doi.org/10.1023/A:1016189724389
30. Landers R, Hübner U, Schmelzeisen R, Mülhaupt R (2002) Rapid prototyping of scaffolds derived from thermoreversible hydrogels and tailored for applications in tissue engineering. Biomaterials 23:4437–4447. https://doi.org/10.1016/S0142-9612(02)00139-4
31. Pfister A, Landers R, Laib A, Hübner U, Schmelzeisen R, Mülhaupt R (2004) Biofunctional rapid prototyping for tissue-engineering applications: 3D bioplotting versus 3D printing. J Polym Sci, Part A: Polym Chem 42:624–638. https://doi.org/10.1002/pola.10807
32. Duarte Campos DF, Blaeser A, Weber M, Jäkel J, Neuss S, Jahnen-Dechent W, Fischer H (2013) Three-dimensional printing of stem cell-laden hydrogels submerged in a hydrophobic high-density fluid. Biofabrication. https://doi.org/10.1088/1758-5082/5/1/015003

33. Bhattacharjee T, Zehnder SM, Rowe KG, Jain S, Nixon RM, Sawyer WG, Angelini TE (2015) Writing in the granular gel medium. Sci Adv 1:e1500655. https://doi.org/10.1126/sciadv.1500655
34. Moxon SR, Cooke ME, Cox SC, Snow M, Jeys L, Jones SW, Smith AM, Grover LM (2017) Suspended manufacture of biological structures. Adv Mater 29:1605594. https://doi.org/10.1002/adma.201605594
35. Rajaram A, Schreyer DJ, Chen DXB (2015) Use of the polycation polyethyleneimine to improve the physical properties of alginate-hyaluronic acid hydrogel during fabrication of tissue repair scaffolds. J Biomater Sci Polym Ed 26:433–445. https://doi.org/10.1080/09205063.2015.1016383
36. Rajaram A, Schreyer D, Chen D (2016) Bioplotting alginate/hyaluronic acid hydrogel scaffolds with structural integrity and preserved schwann cell viability, 3D print. Addit Manuf 1:194–203. https://doi.org/10.1089/3dp.2014.0006
37. You F, Wu X, Chen X (2017) 3D printing of porous alginate/gelatin hydrogel scaffolds and their mechanical property characterization. Int J Polym Mater Polym Biomater 66:299–306. https://doi.org/10.1080/00914037.2016.1201830
38. Sarker M, Izadifar M, Schreyer D, Chen X (2018) Influence of ionic crosslinkers (Ca^{2+}/Ba^{2+}/Zn^{2+}) on the mechanical and biological properties of 3D bioplotted hydrogel scaffolds. J Biomater Sci Polym Ed 29:1126–1154. https://doi.org/10.1080/09205063.2018.1433420
39. Soltan N, Ning L, Mohabatpour F, Papagerakis P, Chen X (2019) Printability and cell viability in bioprinting alginate dialdehyde-gelatin scaffolds. ACS Biomater Sci Eng. https://doi.org/10.1021/acsbiomaterials.9b00167
40. Kim S, Nimni ME, Yang Z, Han B (2005) Chitosan/gelatin-based films crosslinked by proanthocyanidin. J Biomed Mater Res Part B Appl Biomater 75B:442–450. https://doi.org/10.1002/jbm.b.30324
41. Sun J, Tan H (2013) Alginate-based biomaterials for regenerative medicine applications. Materials (Basel) 6:1285–1309. https://doi.org/10.3390/ma6041285
42. Kirchmajer DM, Gorkin R III, Panhuis M (2015) An overview of the suitability of hydrogel-forming polymers for extrusion-based 3D-printing. J Mater Chem B 3:4105–4117. https://doi.org/10.1039/c5tb00393h
43. Lee KY, Mooney DJ (2012) Alginate: properties and biomedical applications. Prog Polym Sci 37:106–126. https://doi.org/10.1016/j.progpolymsci.2011.06.003
44. Munaz A, Vadivelu RK, St. John J, Barton M, Kamble H, Nguyen NT (2016) Three-dimensional printing of biological matters. J Sci Adv Mater Devices 1:1–17. https://doi.org/10.1016/j.jsamd.2016.04.001
45. Sarker MD, Naghieh S, McInnes AD, Ning L, Schreyer DJ, Chen X (2019) Bio-fabrication of peptide-modified alginate scaffolds: printability, mechanical stability and neurite outgrowth assessments. Bioprinting 14:e00045. https://doi.org/10.1016/j.bprint.2019.e00045
46. Habib A, Khoda B (2019) Development of clay based novel hybrid bio-ink for 3D bio-printing process. J Manuf Process 38:12. https://doi.org/10.1016/j.jmapro.2018.12.034
47. Heo DN, Lee S, Timsina R, Qiu X, Castro NJ, Zhang LG (2019) Development of 3D printable conductive hydrogel with crystallized PEDOT:PSS for neural tissue engineering. Mater Sci Eng, C 99:582–590. https://doi.org/10.1016/j.msec.2019.02.008
48. Li D, Zhou J, Chowdhury F, Cheng J, Wang N, Wang F (2011) Role of mechanical factors in fate decisions of stem cells. Regen Med 6:229–240. https://doi.org/10.2217/rme.11.2
49. Williams D, Thayer P, Martinez H, Gatenholm E, Khademhosseini A (2018) A perspective on the physical, mechanical and biological specifications of bioinks and the development of functional tissues in 3D bioprinting. Bioprinting 9:19–36. https://doi.org/10.1016/j.bprint.2018.02.003